NASA Technical Paper 2693

1987

Design, Fabrication, and Performance of Small, Graphite Electrode, Multistage Depressed Collectors With 200-W, CW, 8- to 18-GHz Traveling-Wave Tubes

Ben T. Ebihara
and Peter Ramins

Lewis Research Center
Cleveland, Ohio

National Aeronautics
and Space Administration

Scientific and Technical Information Branch

Summary

Small multistage depressed collectors (MDC's) which used pyrolytic graphite, ion-beam textured pyrolytic graphite, and isotropic graphite electrodes were designed, fabricated, and evaluated in conjunction with 200-W, continuous wave (CW), 8- to 18-GHz traveling wave tubes (TWT's). The design, construction, and performance of the MDC's are described. The bakeout performance of the collectors, in terms of gas evolution, was indistinguishable from that of typical production tubes with copper collectors. However, preliminary results indicate that some additional radiofrequency (RF) and dc beam processing time (and/or longer or higher temperature bakeouts) may be needed beyond that of typical copper electrode collectors. This is particularly true for pyrolytic graphite electrodes and for TWT's that do not have appendage ion pumps. Extended testing indicated good long-term stability of the textured pyrolytic graphite and isotropic graphite electrode surfaces. The isotropic graphite in particular showed considerable promise as an MDC electrode material because of its high purity, low cost, simple construction, potential for very compact overall size, and relatively low secondary-electron-emission yield characteristics in the as-machined state. However, considerably more test experience is required before definitive conclusions on its suitability for electronic countermeasure systems and space TWT's can be made.

Introduction

An investigation of secondary-electron-emission losses in MDC's, summarized in reference 1, showed that these losses are significant, and that a substantial improvement in the overall efficiency can be obtained with the use of carbon MDC electrode surfaces in place of the machined copper surfaces generally used. That investigation, in which demountable MDC electrodes were operated in a large vacuum system, was concentrated on TWT and MDC efficiency measurements and comparisons. Other important concerns for practical MDC electrodes, such as long-term surface stability, outgassing characteristics, and fabrication technology, were not explored.

These concerns were addressed in a separate investigation, which involved small TWT-MDC vacuum envelopes and complete collector assemblies. This ongoing investigation covered fabrication technology of pyrolytic and isotropic graphite electrode MDC's, MDC bakeout requirements, MDC outgassing and TWT-MDC RF-dc beam processing requirements, and long-term electrode surface stability. A number of small, complete prototype MDC assemblies were built and tested, with the existing TWT's used in the demountable MDC tests. This investigation led eventually to the design, fabrication, and evaluation of a number of graphite MDC's mounted on 200-W, CW, 8- to 18-GHz TWT's.

The MDC geometric design was produced by using a recently developed, computer-aided design technique for TWT's that uses MDC's and permanent magnet spent-beam refocusers. This technique, as well as a comparison of computed and measured TWT-MDC performance, is described in reference 2.

The present paper describes the following:

(1) Design and fabrication of the graphite MDC assemblies
(2) Bakeout performance of the collectors
(3) MDC outgassing and RF-dc beam processing of the collectors
(4) TWT-MDC performance with the graphite collectors over a range of operating conditions
(5) MDC performance and electrode surface stability over a longer period of time

This investigation was part of a program to improve the performance of TWT's for use in communication and electronic countermeasure (ECM) systems, conducted jointly with the U.S. Air Force.

The authors wish to express their gratitude to A.N. Curren of the NASA Lewis Research Center for the ion texturing of the pyrolytic graphite MDC and scanning electron microscope examinations of the textured electrode surfaces.

Symbols

f	operating frequency, GHz
I_{en}	current to n^{th} collector electrode, mA
I_G	total current to TWT body (ground), mA
I_0	cathode or beam current, mA
P_b	sum of beam interception losses and circuit losses, W
P_{RF}	total RF output power, W
P_{rec}	recovered power in collector, W
V_{en}	voltage on n^{th} collector electrode, with respect to ground, V
V_0	cathode voltage with respect to ground, V

η_{ov} overall TWT efficiency,

$$\frac{P_{RF}}{\sum_{n=1}^{4} (V_0 - V_{en})I_{en} + I_G V_0}, \text{ percent}$$

η_{RF} RF efficiency, $P_{RF}/V_0 I_0$, percent

Design, Fabrication, and Performance Evaluation Program

Overall Program

The program included the design, fabrication, and performance evaluation of small, four-stage, graphite electrode collectors in conjunction with four CW TWT's (Varian Assoc., Inc. (VA) model VTM-6294). The MDC's were designed and fabricated at NASA Lewis Research Center. The design effort included both the active section (electrode geometry) and the passive electrode support structure (including cooling, high-voltage (HV) standoff, and vacuum envelope designs) of pyrolytic and isotropic graphite versions of the same basic MDC type.

The MDC's were joined to the TWT bodies, baked out, and focused at Varian, Microwave Tube Division. In the cases of TWT 202 and 204, where no unusual problems were encountered and the pulsed RF-dc beam processing (outgassing) time was not excessive, the TWT-MDC's were brought up to CW operation before shipping them to Lewis. The bakeout performance, early collector HV standoff characteristics, and early RF-dc beam processing (outgassing) performance were noted in a log supplied by Varian with each TWT. The optimization and evaluation of the TWT-MDC performance, including some longer term testing of the stability of the collector electrode surfaces, were performed at Lewis.

TWT and MDC Characteristics

The general characteristics of VA model VTM-6294 are shown in table I. The geometry of the active portion of the MDC and typical operating potentials are shown in figure 1. The electrode materials and surface characteristics are summarized in table II. The technique used to ion-beam texture the pyrolytic graphite electrodes of TWT 203 is described in reference 3.

TABLE I.—GENERAL CHARACTERISTICS OF VARIAN TWT MODEL VTM-6294

Frequency, f, GHz	8 to 18
Cathode voltage, V_0, kV	9.4 to 9.8
Cathode current, I_0, A	0.24
Perveance, $A/V^{3/2}$	0.26×10^{-6}
RF efficiency, η_{RF}, percent	15 (maximum)
Focusing	Periodic permanent magnet (PPM)
Duty cycle, percent	100

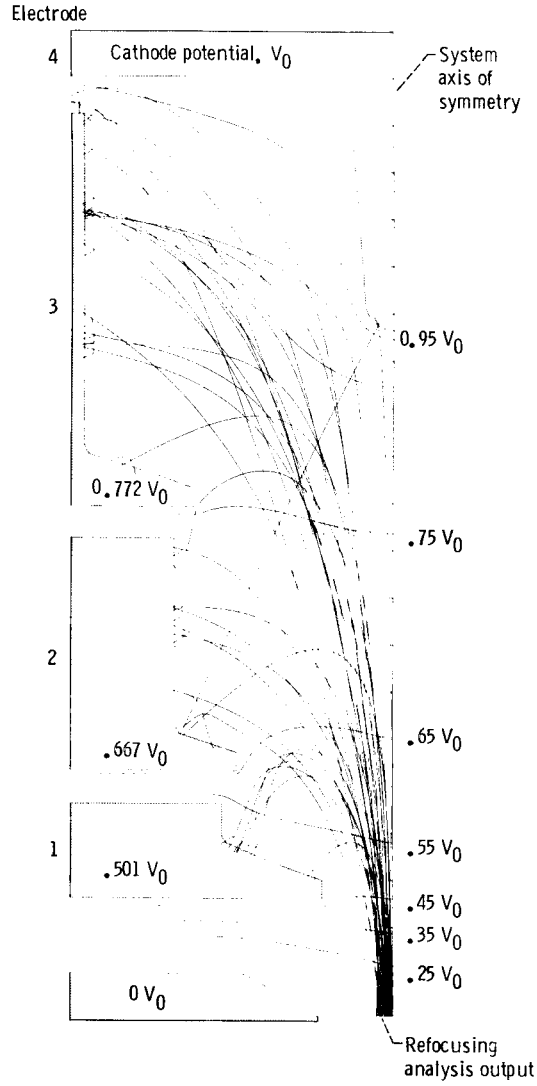

Figure 1.—Electrode geometry, typical applied potentials, and charge trajectories in four-stage, 1.7-cm-diameter depressed collector.

TABLE II.—SUMMARY OF MDC ELECTRODE MATERIALS AND SURFACE CHARACTERISTICS

TWT serial number	MDC electrode material	MDC electrode surface characteristics
201	Pyrolytic graphite	Bead blasted (C-direction surfaces only)
202	Pyrolytic graphite	Machined
203	Pyrolytic graphite	Ion-beam textured
204	Isotropic graphite	Bead blasted

MDC Design Requirements

The outer housing of the MDC was made of a welded, all-metal shell (except for the electrical feedthroughs) that served as a vacuum barrier (operating at ground potential) and as a surface for cooling the collector conductively. This avoided the use of ceramics as a vacuum barrier and ceramic-to-metal brazes as vacuum seals. However, ceramics were used within the housing to isolate the electrodes operating as high as −10 kV from ground.

The maximum allowable diameter of this shell was 4.6 cm so that it could be fitted within the volume of the existing production TWT-MDC package. This requirement for the passive pyrolytic graphite electrode support structure constrained the active (graphite) size of the MDC to 1.7 cm outer diameter. The collector body was required to dissipate as much as 400 W of power with the graphite electrodes operating below the bakeout temperature. In the worst case (operation with the dc beam), this power was dissipated on a single (third-stage) electrode.

At the start of this program, only pyrolytic graphite MDC's were planned. However, when promising results were obtained with other isotropic graphite MDC's (ref. 1), an isotropic graphite MDC was designed and built for TWT 204.

MDC Assembly Design and Fabrication

Basic Electrode Materials

The electrodes for the collectors were made from either pyrolytic or isotropic forms of graphite. Some of the salient properties of the two forms of graphite are shown in table III, and their relative merits are found in table IV. As a precautionary measure, both graphites were vacuum-baked at 1900 °C before brazing to insure purity.

Pyrolytic graphite.—Pyrolytic graphite (PG) is a highly anisotropic, brittle but machinable material having adequate strength and purity. The material was available from at least three different sources in the United States. Pyrolytic graphite is manufactured by a chemical deposition process wherein carbonaceous gas undergoes pyrolysis at extremely high temperatures and deposits out in dense, orderly layers to form a material with a laminated structure. The unique properties of PG arise from its high degree of preferred crystalline orientation and its atomic structure (ref. 4). The crystallographic planes of PG are defined by the *AB*-planes, which are parallel to the deposition layers. The *C*-direction is perpendicular to the *AB*-plane. The surfaces exposed by cutting in the *C*-direction are referred to as the "*C*-surface" in this report (see sketch on table III).

The high anisotropy of PG is due to the large differences in the bonding strengths of the atoms within and between the crystallographic planes. Parallel to the *AB*-planes, where the covalent, atomic-bonding forces are very strong, PG exhibits high strength and high thermal conductivity but extremely low

TABLE III.—SOME PROPERTIES OF PYROLYTIC AND ISOTROPIC GRAPHITES

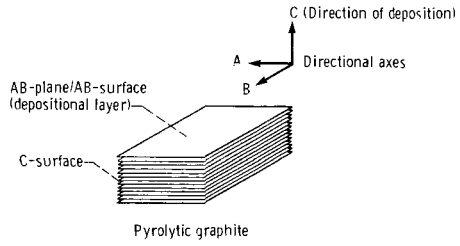

Property	Pyrolytic graphite[a]		Isotropic graphite[b]
	AB-plane	*C*-direction	
Tensile strength at room temperature, Pa (psi)	9.65×10^{7} (14 000)	2.76×10^{6} (400)	5.52×10^{7} (8 000)
Compressive strength at room temperature, Pa (psi)	6.89×10^{7} (10 000)	3.10×10^{8} (45 000)	1.31×10^{8} (19 000)
Thermal conductivity, cal/cm^2 cm sec C	0.827	0.004	0.289
Coefficent of themal expansion at room temperature, cm/cm C	1.8×10^{-6}	23.4×10^{-6}	7.7×10^{-6}
Density, g/cm^3	2.20 (2.265 theoretical)		1.84
Particle size, μm	———		25
Average pore size, μm	———		0.4
Porosity, percent	3		19

[a]From reference 4.
[b]From POCO Data Sheet.

TABLE IV.—RELATIVE COMPARISONS OF PYROLYTIC AND ISOTROPIC FORMS OF GRAPHITE

Characteristic	Pyrolytic graphite[a]		Isotropic graphite[b]
	AB-plane	*C*-direction	
Secondary-electron yield	Fairly low	Low[a]	Low
Thermal conductivity	Excellent (≈ copper)	Poor (1/300 copper)	Fair (1/3 copper)
Thermal expansion	Very low (≈ 0)	Very high (> copper)	Medium (≈ alumina)
Tensile strength	Good	Poor	Good
Thermal emissivity	Good	Very good[a]	Very good
Brazeability	Poor	Good[a]	Good
Structure	Preferred crystalline orientation		Agglomeration
Impurities, ash content	100 ppm		5 ppm
Machinablity	Good		Very good
Outgassing	Slow		Fast
Material cost (approx.), dollars/electrode	50		5
MDC size	Small		Smaller

[a]C-surface as defined in table III

thermal expansion. However, in the *C*-direction, where the layers are held together by weak, nonvalent, residual type bonding (sometimes referred to as van der Waals forces), such properties are the reverse.

The PG electrodes were used in an orientation where the electrons were collected mostly on the *C*-surfaces, noted for their low secondary electron yield (ref. 3). In figure 2, the vertical inner diameters of the PG collector electrodes are *C*-surfaces, while the upper surfaces of the apertures are

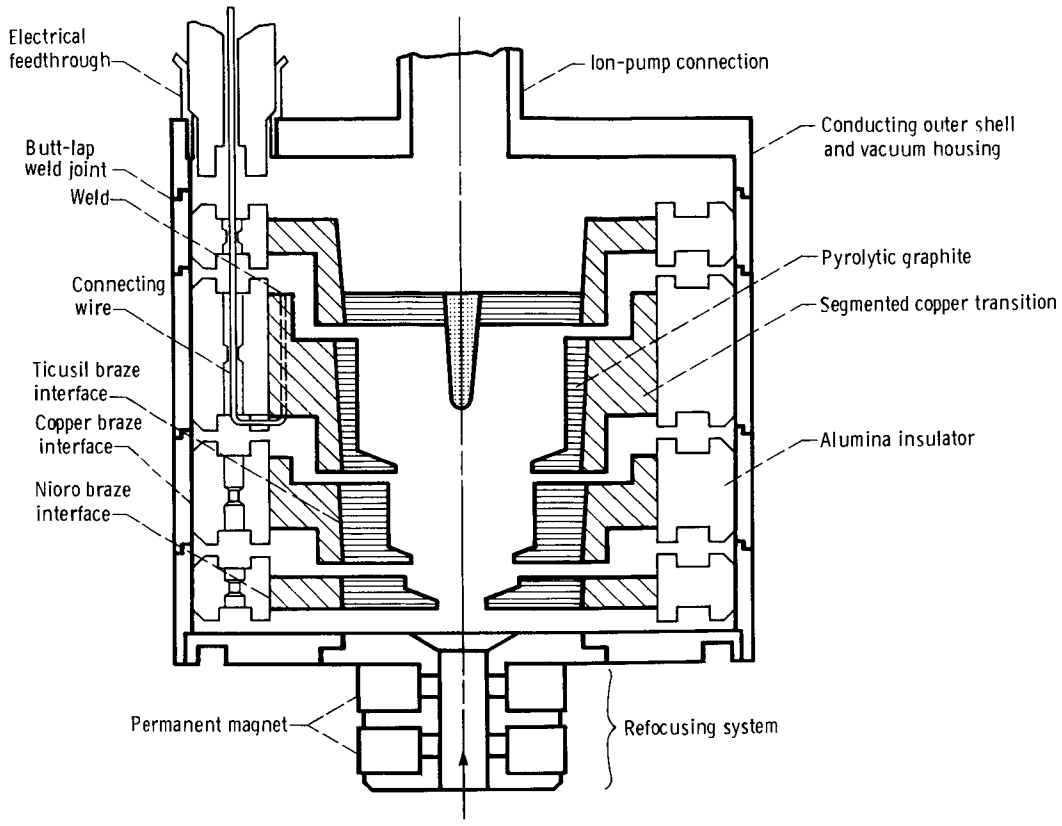

Figure 2.—Cross section of four-stage, brazed, pyrolytic graphite electrode depressed collector and permanent magnet refocusing system. Striated markings symbolize the pyrolytic graphite layers along the *AB*-plane. The *C*-direction is perpendicular to the *AB*-plane.

combinations of *AB*- and *C*-surfaces. The top and bottom of each electrode are *AB*-surfaces. Heat is moved by conduction along the highly conductive *AB*-plane. The electrodes were made from thick, flat PG plates supplied by Pfizer Minerals, Pigments and Metals Division, Easton, Pennsylvania. The material was free of visible cracks and delaminations.

Isotropic graphite.—A great number of graphites are available with physical characteristics that vary widely over a considerable range. These characteristics are determined basically by the carbon-based starting material, the particle size and shape, and the nature of the graphite manufacturing processes. The properties of graphite particles are inherently anisotropic. If the particles are flakelike in shape, any compaction process causes preferential alignment of the flakes and imparts directional characteristics to the material. However, a structure having virtually isotropic properties can be produced if the particles are in the form of spherically shaped grains so that their randomly oriented positions are not disturbed. POCO Graphite, Inc., among others, manufactures isotropic graphites by using their own proprietary technology. The collector electrodes were made from POCO's purified grade DFP-2 isotropic graphite, which is a fine-grained, high-purity, easily machinable material having other distinctive advantages as well (Data Sheet for DFP-2, Semiconductor/Metallurgical Grades, POCO Graphite, Inc., Decatur, Texas, Jan. 1, 1978). The material has an open and interconnecting porosity, which expedites outgassing during vacuum bakeout. Its coefficient of thermal expansion is such that direct brazing to alumina is possible. The impurity level of less than 5-ppm ash content is 20 times less than the pyrolytic graphite that was used. A light bead-blasting of the electrode surface made from this material helped in reducing secondary-electron-emission yield (ref. 1).

Design Concepts

Description of construction techniques.—A unique construction technique was devised in order to satisfy the various requirements discussed in the subsection MDC Design Requirements (ref. 5). The photographs in figures 3 and 4 show the modular assembly techniques used for the fabrication of the collectors. Figures 2 and 5 reveal a more detailed view of the interior designs. The basic modular design was suitable for the MDC construction with the two different types of graphite electrodes, although there was an added complexity to the fabrication of the PG electrodes because of the requirement for transition spacers.

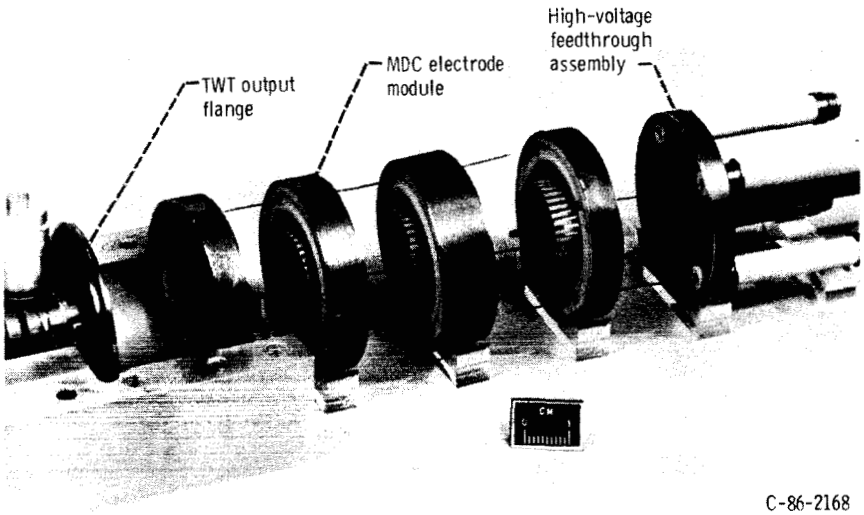

Figure 3.—Four-stage, pyrolytic graphite electrode depressed collector detached from TWT and separated at each of the welded junctions after completion of testing.

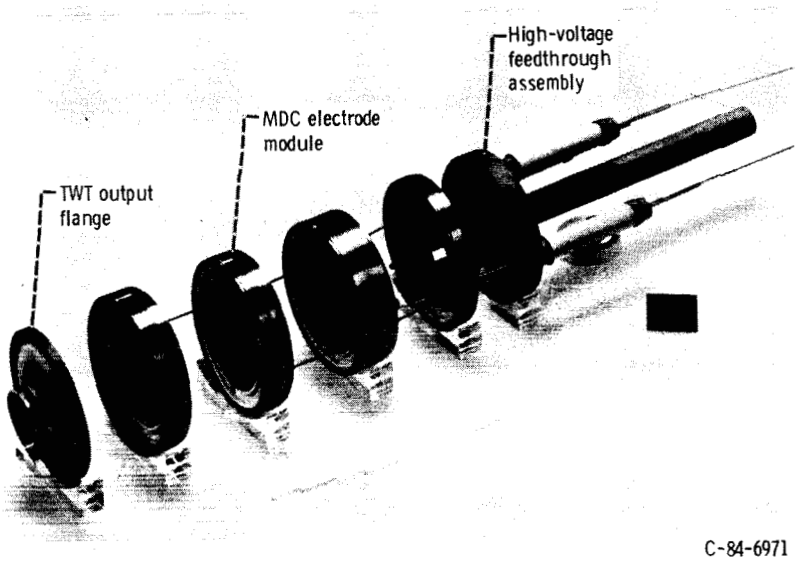

Figure 4.--Exploded view of four-stage, isotropic graphite electrode depressed collector ready for final assembly by welding.

There were advantages to having the electrode modules in loose or separable pieces. This structure provided maximum accessibility to the electrode such that further modification to the surfaces such as ion-beam texturing was feasible. Since the final machining of the electrodes was performed while the electrodes were supported in the modules, accurate control over their dimensions, spacings, and alignments was possible. This procedure also allowed the flexibility to replace, bake, high-voltage test, and/or clean any module up to the time of final closure by welding.

Figure 6 shows how each module, representing a single electrode, was built as a brazed composite unit with a centrally located graphite electrode, which was electrically isolated with a ceramic ring from the thin metal outer sheath. An additional component, a segmented copper transition ring, was required to retain the PG electrode because of anisotropic thermal expansions (discussed in the subsection Supporting Components). Such a transition part was not needed for the retention of isotropic graphite (fig. 7).

The modules were stacked to create a multiple-tiered arrangement of electrodes (figs. 2 and 5). After electrical connections were made internally between the electrodes and to the respective electrode terminals, the modules, together with the end plates, were joined by welding the edges of the sheaths to form a vacuum-tight, integrated collector package (fig. 8).

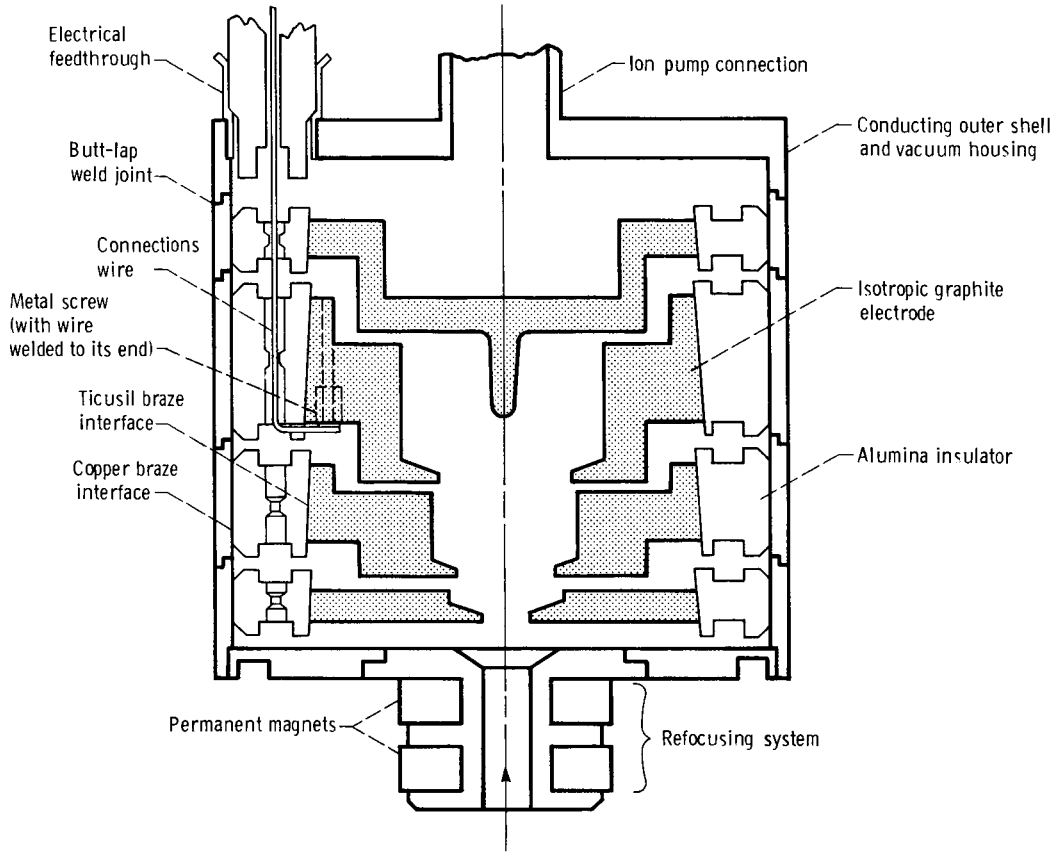

Figure 5.—Cross section of four-stage, brazed, isotropic graphite electrode depressed collector and permanent magnet refocusing system.

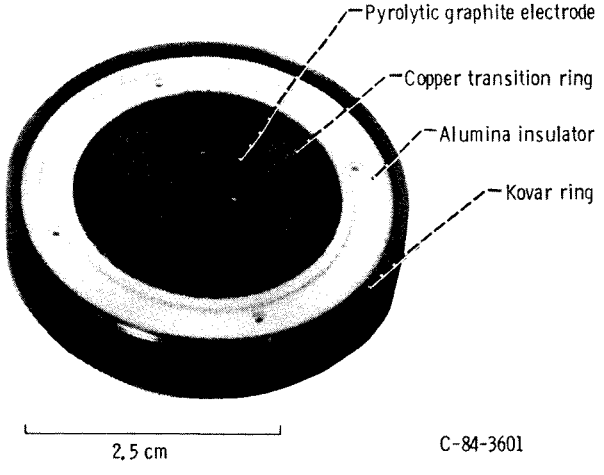

Figure 6.—Typical all-brazed electrode module showing pyrolytic graphite electrode, segmented copper transition, alumina insulator, and Kovar-metal outer ring.

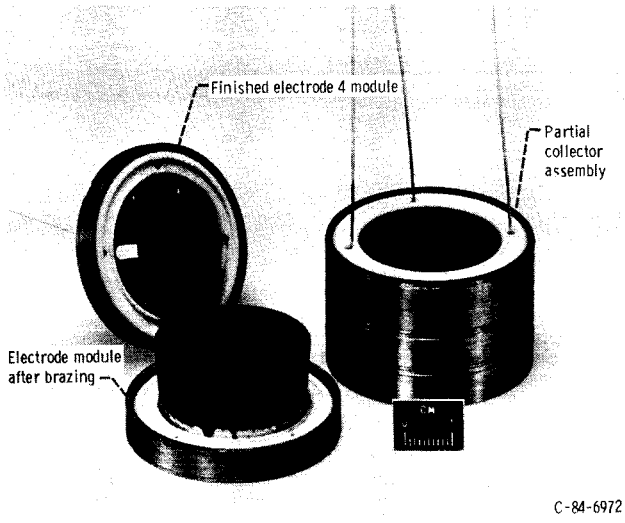

Figure 7.—Set of modules for four-stage, isotropic graphite electrode depressed collector. Partial collector assembly includes three electrode-modules, electrically wired and ready for welding at the joined edges.

Mechanical and thermal integrity.—The collector (or its subassemblies) was subjected to several high-temperature brazing cycles at tempeatures between 900 to 1100 °C and a long bakeout period at temperatures up to 550 °C. During the testing phases, the collectors experienced numerous thermal cycles, at lower temperatures, as a result of pulsing and on/off cycling.

Since collectors cannot avoid thermally induced stresses, it was essential that, wherever possible, the collector components have closely matched coefficients of thermal

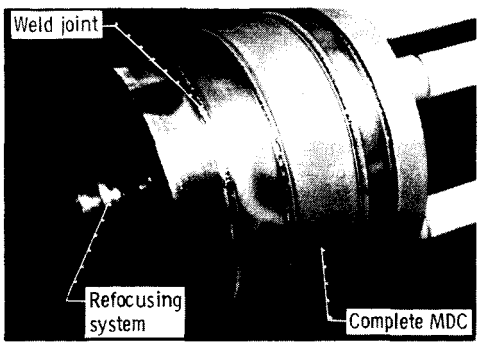

Figure 8.—Collector assembly shown with electrode modules stacked and electron beam welded but without finish machining of the outer diameter.

expansion. In cases where that was not feasible two techniques were employed. One was to use the ductile deformation of copper to relieve stresses. The other was to offset the movements of the low-expansion pyrolytic graphite (*AB*-plane) with a high-expansion material (copper).

Joining Methods

Brazed joints.—Brazing was the only expedient method for joining collector components made of various materials. Since brazed interfaces fill joint gaps, they provide the most efficient means of removing heat in vacuum by conduction from the electrodes to the outer wall of the collector, and they serve to eliminate virtual leaks. Brazed joints provide the structural integrity under operating conditions of changing temperatures and vibrations. They also prevent the release of loose carbon particles that usually evolve from the abrasive action of mechanically fastened joints due to expansion/contraction movements. These carbon particles may be a potential problem in collectors deployed in zero gravity.

Braze filler metal.—There are problems that must be addressed and solved before brazing can be accomplished successfully. Most conventional braze alloys will not wet either graphite or alumina. Also, no braze alloy can effectively join two materials having wide differences in thermal expansions, much less the anisotropic expansion found with PG.

A survey conducted by Hughes Aircraft Co., under NASA contract, revealed several potential braze alloys suitable for joining graphites (ref. 6). One of these, Ticusil, an active-metal braze material, produced excellent bonding with both graphite and alumina when brazed in a vacuum furnace. Generally, brazes containing active-metal constituents (elements such as titanium, zirconium, chromium, and tantalum that form strong carbides) will wet graphites. Braze ductility should not be overlooked. When brittle materials such as isotropic graphite and alumina are joined, the ductility of a braze alloy through deformation helps to relieve excessive thermally induced stresses.

Ticusil (68 percent silver, 27 percent copper, and 5 percent titanium), as used, was not an alloy but a laminated sheet with a pure titanium foil sandwiched in the center. According to H. Mizuhara of Wesgo Division, GTE Products Corp., Ticusil remains ductile because full alloying does not take place at the low, short-duration brazing temperature of 900 °C.

Brazing was most effective when the Ticusil foil was placed in direct contact with the graphite surface prior to brazing. A cylindrical surface was brazed in this way by preparing a tapered joint interface where a braze foil was placed between the graphite and its mating part. It was necessary to apply a slight pressure at the interface during brazing to obtain a void-free braze joint.

Multiple-brazing operations.—The PG electrode modules required three separate brazing operations. A copper braze was performed first at the interface between the metal sheath and the metallized alumina. The next braze run, made with a gold-nickel braze (82 percent gold and 18 percent nickel), joined the metallized inside diameter of the alumina to the copper transition part. The final braze, made with Ticusil, joined the graphite to the copper transition part.

The isotropic graphite collector module, which consisted of three parts, required only two brazing operations. The first one joined the sheath to the alumina with a copper braze similar to that for the PG collector. The second one used Ticusil to join graphite to the unmetallized alumina (fig. 7).

Strength of PG braze joint.—A tensile strength test fixture was made as shown in figure 9 to test the tensile strength of the Ticusil-brazed interface joining PG to copper. The joint also simulated the actual transition joint bonding the *C*-surface of PG. The results of the test indicated that the joint was stronger than the bulk material. However, the failure occurred at a low stress level that was one-sixth of the rated value of PG. Brittle fracture is difficult to explain because of the unknown effects of residual stresses, flaws, and crack propagation factors.

Quality of isotropic graphite braze interface.—Figure 10 shows a good braze joint and an interesting braze interface made between isotropic graphite and unmetallized alumina. A braze foil was placed in the joint between the two materials before melting. With Ticusil braze alloy, it was not necessary to premetallize either alumina or graphite to achieve bonding. The holding power of the braze appears to be augmented by the wetting action and the penetration of Ticusil into the pores of the graphite.

Welded joints.—The edges of the outer ring on each of the electrode modules and the feedthrough plate were prepared with matching butt-lap joints to provide self-fixturing weld connections and concentric alignment of the electrodes. After the modules were wired internally and stack assembled, single-pass, half-penetration, electron-beam welds were made to seal the lap joints (fig. 8). A full-penetration weld might have ejected or sputtered materials inside the collector and risked contamination of the insulator surfaces. A narrow, low-

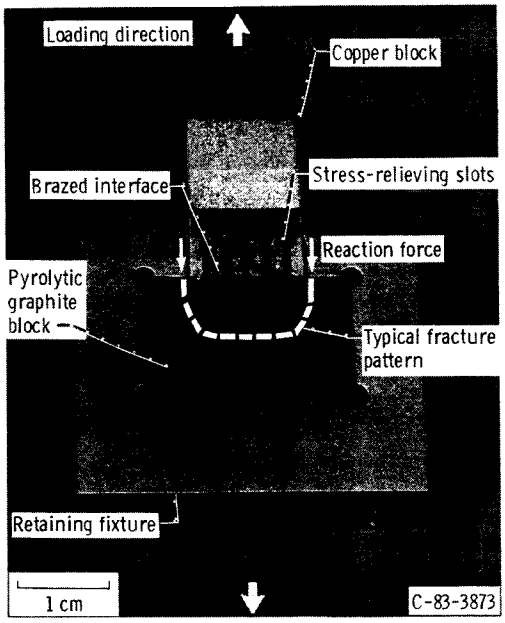

Figure 9.—Tensile test fixture retaining a block specimen of pyrolytic graphite brazed to copper. Slots machined in the copper are for relieving differential contraction stresses from brazing temperature.

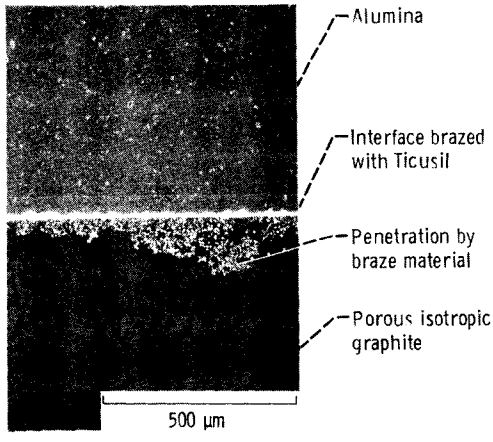

Figure 10.—Cross section of brazed interface between alumina and isotropic graphite.

penetration weld was easily accomplished with the electron beam. Its low heat input prevented excessive heating of the nearby ceramic-to-metal copper braze joint. Even then, as an extra precaution, copper heat sinks were installed next to the weld joints to prevent overheating by the welding process.

Supporting Components

Transition spacer.—Pyrolytic graphite has an unusual anisotropic coefficient of thermal expansion that varies from almost zero parallel to the *AB*-plane to a high value, exceeding that of copper, in the *C*-direction. The difficulty of retaining such a material was resolved by the design and usage of a segmented, copper transition ring which was interposed between the alumina insulator and the PG electrode. The copper was slotted to create flexible, easily deformable, stress-relieving segments that tightly connected the ceramic to the graphite. This configuration provided a good heat transfer path as well as a reliable method to retain and support the PG electrode. The combined effects of segmentation and deformation allowed the three brazed members to move without encountering high, damaging stresses. However, more than ductile deformation was required for handling the thermal movements in the radial directions. This need was satisfied by the proper sizing of the segment lengths by equating the combined thermal expansions of the copper transition and the graphite electrode (*AB*-plane) to that of the encircling alumina.

Figure 11 shows a typical transition part. Stopping the radial slots just short of the inside diameter produced a continuous brazing surface and provided a method for holding all the segments together.

Although the wide variations in the thermal expansion coefficients of the PG and alumina being joined by brazing necessitated the use of a transitional spacer, there was no such need in the construction of the isotropic electrode collector. A suitable graphite, having a uniform expansion coefficient which matched closely that of the connecting alumina, was used so that direct brazing of these two materials was possible.

The simplification achieved with the elimination of the transition part gave the isotropic electrode MDC a definite advantage over a PG electrode MDC. In addition to the cost

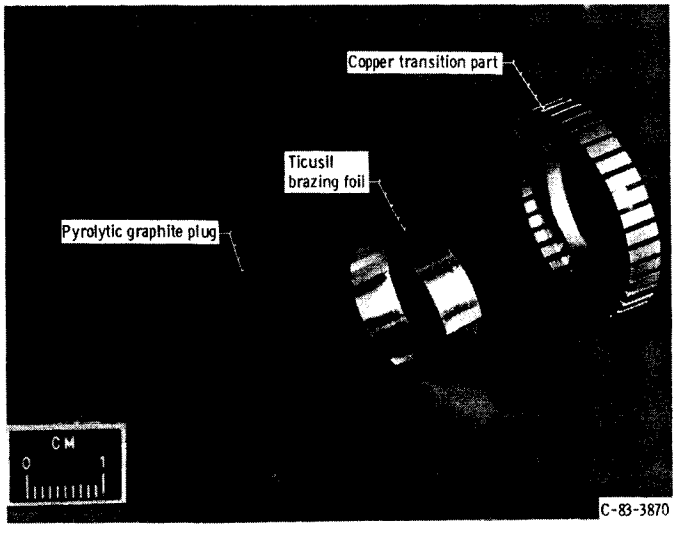

Figure 11.—Parts for pyrolytic graphite electrode collector.

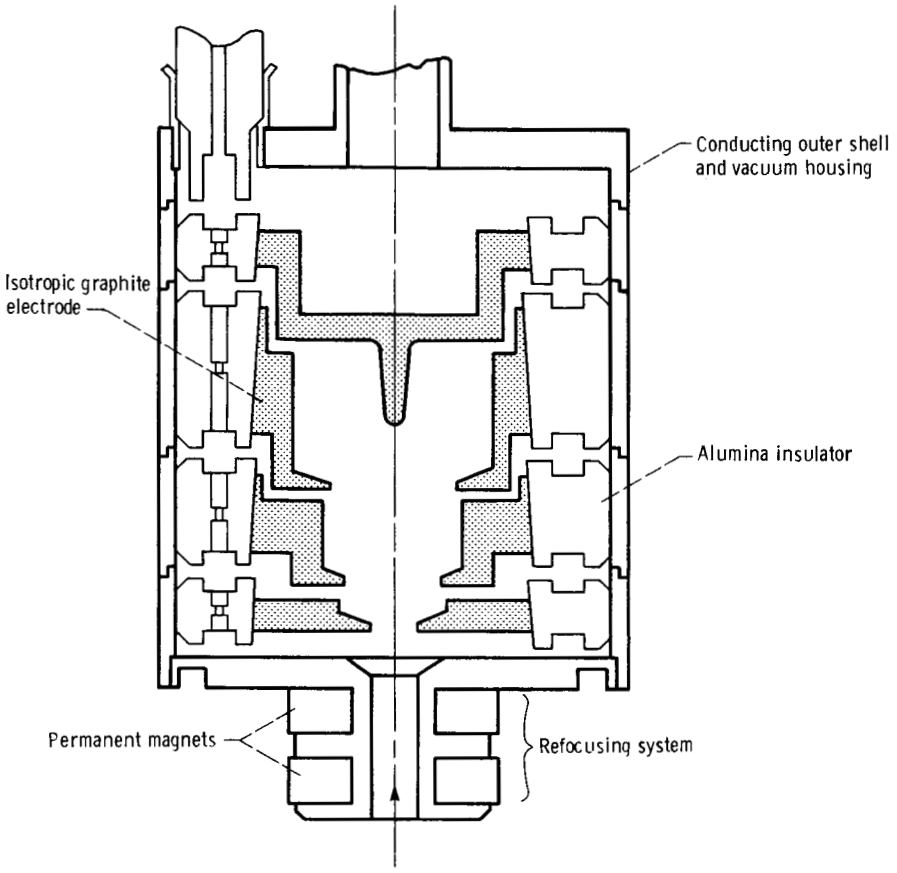

Figure 12.—Cross section of same collector shown in figure 5, drawn to same scale, but having less volume of graphite to achieve reduction in shell diameter.

saved by not fabricating the part and by having one less brazing operation, it is possible to reduce the overall diameter of the collector body (fig. 12). The actual isotropic graphite collector built had the same body size as the collector in figure 5 for the practical expediency of making the least number of changes and using existing parts. However, the collector was larger than necessary, and as a result a greater volume of graphite material was used than was essential.

Electrical insulators and connections.—Alumina insulators, made from Wesgo Al-300 material, were used to isolate the electrodes, which were maintained at high negative potentials from the grounded outer metal shell and from each other. Heat passed through the alumina to reach the outer wall of the collector. Alumina, in spite of its poor thermal conductivity, was used because of its nontoxic nature. Beryllia, which has seven times the thermal conductivity of alumina, would be an excellent replacement in high-power, production-model TWT's.

The alumina ceramics were grooved on the top and bottom surfaces to obtain longer surface breakdown paths for minimum insulator thickness, which was necessary to aid heat conduction. A maximum value of 10 kV/cm was used for the design of the path length to prevent high-voltage surface breakdown.

To make a more compact collector, the wires were passed through holes drilled in the alumina insulators. These wires were attached to their respective feedthroughs located on the top of the collector. Since the electrical standoff of the feedthroughs was marginal because of internal construction, the wires were sheathed with thin alumina tubes.

Metal containment.—The distortions and movements that usually occur during brazing could affect accurate positioning of the electrodes. Therefore, the final machining of the electrode plugs was done after completion of all braze operations. The outer metal rings surrounding each module provided the necessary locating surfaces in both the radial and axial directions for the subsequent machining of the electrode configurations. After the edges of these sheath rings were joined together by welding, they formed the necessary vacuum barrier, the main structural support, and the cooling wall for the collector.

The metal rings were made of Kovar, an iron-nickel-cobalt alloy, because Kovar's thermal expansion closely matches the

thermal expansion of the adjoining alumina at temperatures up to 650 °C. However, above that temperature, Kovar's expansion rate exceeds that of alumina. To constrain Kovar's overexpansion at high temperatures and to maintain the tight clearances necessary for brazing, a restraining molybdenum ring keeper was used. The keeper allowed Kovar to be brazed successfully to the alumina by using a copper braze. With braze alloys containing silver, Kovar becomes sensitive to stress-corrosion cracking, and there is an increased risk of vacuum leakage.

Shielding of insulators.—Two methods were employed to protect the insulators from electron bombardment and to reduce contamination. One method was to offset the gap between the ceramic insulators with respect to the electrode openings. The step, or jog, shown in the transition part of figure 2 and in the electrode of figure 5 prevented line-of-sight electron impingements on the insulators. The chamfers and grooves machined into the insulators, primarily intended for lengthening the voltage breakdown path, provided partial shielding from electrically conductive deposits.

Performance Evaluation and Optimization Techniques

The TWT bodies were added to the MDC's without any previously documented TWT performance with undepressed collectors. Consequently, the TWT body losses were unknown, and the MDC efficiencies could not be computed from measured quantities (ref. 1). Estimation of collector efficiencies, based on assumed values of beam interception and circuit losses, was not attempted because the large observed differences in the basic performance of individual TWT's of this model (discussed later in this section) precluded any meaningful comparisons of collector performance with the various electrode surfaces.

TWT-MDC performance optimization was limited to optimization of the MDC operating voltages for broadband operation. Optimization of the refocusing system by trimming the strength of the two permanent magnets was not attempted, since very good results were obtained at the nominal values (ref. 2).

Filtered input drive at the fundamental frequency was used throughout these tests. Saturation was determined by using an uncalibrated power meter which, by means of a low-pass filter, measured RF power only at the fundamental frequency. However, only the total RF power P_{RF} (including any harmonic power) that was dissipated in the water-cooled matched load was measured, and all TWT overall and electronic efficiencies reported here are based on this P_{RF}.

Results of Bakeout, HV Testing, and Processing

TWT 201 and Pyrolytic Graphite MDC

Following a 44-hr bakeout at 500 °C the TWT-MDC went back to atmospheric pressure because of one or more leaks in the TWT body. After the second bakeout, 38 hr at 475 °C, large electrical leakage across the MDC electrode insulators (to ground) was observed. In terms of outgassing performance the TWT-MDC was indistinguishable from production TWT's. After the TWT beam was focused, the TWT was tested very briefly at VA at low duty cycle with the MDC electrodes essentially undepressed and then delivered to Lewis.

Following a few months of storage, with the ion pump operating, the electrical leakage was considerably smaller, and the MDC could be operated at the nominal voltages with tolerable leakage. This steady-state leakage was subtracted in subsequent testing by using differential sample and hold circuits, which sampled the MDC electrode current during times when the TWT was pulsed on and off.

TWT 201 was the last one of the TWT's to be tested and had been in storage with the ion pump on for about 1 yr. The TWT was brought up to CW operation in about 3 hr with very little outgassing observed. The 2-l/s ion pump current peaked at 0.27 μA and dropped quickly (over minutes) to less than 0.1 μA, and then more slowly to 0.01 to 0.02 μA after a total of about 150 hr of CW operation.

With CW operation, the total body current I_G rose slowly by several milliamperes after turn-on and persisted for a time after the tube was turned off. This effect was considerably larger for operation with the dc beam. This was attributed to increased electrical leakage across the MDC insulators as the parts reached operating temperature. Consequently, the TWT-MDC performance was optimized and obtained only under pulsed conditions, where the differential sample and hold circuits could be used to subtract out the nonsteady electrode leakage currents.

Because the electrical leakage in the MDC persisted (and seemed to be getting worse) the testing was terminated, and the MDC was cut apart. Examination of the parts indicated that the leakage was due to a buildup of conducting deposits on the HV feedthroughs. These deposits apparently came from constituents in the braze alloy used with this particular feedthrough assembly that vaporized at high temperatures. Other supposedly identical feedthroughs purchased at the same time did not exhibit such electrical leakage after a high-temperature bakeout. For example, TWT 204 (discussed in the subsection TWT 204 and Isotropic Graphite MDC) exhibited no electrical leakage after a higher (550 °C) temperature bakeout. The MDC ceramics of TWT 201 were clean and exhibited no leakage.

TWT 202 and Pyrolytic Graphite MDC

Because of the difficulties encountered at Varian with TWT 201, the bakeout temperature of TWT 202 was lowered to 450 °C. The duration was 56 hr. MDC electrode electrical leakages (to ground) of fractions of a milliampere, at the rated operating voltages, were observed right after the bakeout. These leakages decreased to zero after some time. The TWT-MDC was brought up to CW operation at Varian after slightly more than 100 hr of pulsing. The 2-l/s pump current was approximately 0.1 μA after 24 hr of CW RF aging. A set of TWT-MDC data was obtained at Varian at saturation across the operating band of 8 to 18 GHz, but shortly afterwards the TWT experienced a shutdown. Subsequently, the tube evolved a considerable amount of gas and required a return to pulsed operation. Furthermore, the voltage on collector electrode 3 had to be reduced more than 500 V to keep I_G at previous levels. The TWT was then shipped to Lewis. The problem was later diagnosed to be a partial separation of the metallized coating joining the ceramic and copper of electrode 3. Consequently, although the TWT was extensively tested later at Lewis under CW conditions, electrode 3 was operating far above the design temperature because of the reduced heat transfer across the separated portion of the braze joint and increased thermal dissipation due to the reduced operating voltage. The persistent (but relatively low level) outgassing that occurred throughout the test program can be attributed to this problem.

TWT 203 and Textured Pyrolytic Graphite MDC

The TWT was baked for 30 hr at 450 °C. Following the bakeout, collector electrodes 1 to 3 showed an electrical leakage to ground of several milliamperes even at applied potentials significantly lower than the design voltages. A failure report was submitted by Varian. The TWT beam was focused at low duty cycle ($\leq$2 percent), and the testing was very limited prior to shipment to Lewis. After 2 weeks of storage, the largest leakage was less than 20 μA at the nominal operating voltages. Leakages of this magnitude persisted to the end of the test program.

Because of the delicate nature of the textured carbon electrode surfaces (which could be damaged by arcing) the TWT-MDC was outgassed rather thoroughly under pulsed conditions. Approximately 180 hr of pulsed operation, probably considerably more than actually required, was accumulated before going to CW operation. Pump current was only 0.1 μA at the start of CW operation. After about 20 hr of CW operation, the TWT could be operated without the ion pump with little if any gas accumulation as long as steady operation was maintained. However, following some unplanned shutdowns due to power supply failures significant gas evolution was observed. Moreover, when the TWT operating condition was changed radically after a longer time of steady-state operation (e.g., going to dc beam after days of operation at saturation or vice versa), a very significant amount of outgassing was observed. This outgassing lasted only for a relatively short time (seconds or minutes), but it was sufficiently high to pose some risk of arcing. This behavior persisted to the end of the 2000-hr extended test program.

TWT 204 and Isotropic Graphite MDC

The TWT was baked out at 550 °C for 30 hr. As was the case for the pyrolytic graphite collectors, the bakeout performance of this isotropic graphite MDC was indistinguishable from the production TWT's with copper collectors. Following the bakeout the MDC exhibited tens of microamperes of electrical leakage at the nominal operating voltages. This leakage had disappeared entirely by the time the TWT was delivered to Lewis.

Approximately 35 hr of pulsed dc aging (no RF) and over 30 hr of gradual, CW, RF aging were required (at Varian) before saturated CW data could be obtained across the useful operating band.

During initial testing at Lewis, the 2-l/s ion pump was used continually. Pump currents, which ranged from 0.02 to 0.025 μA initially, dropped to virtually zero ($<$5 to 10 nA, the minimum detectable on the pump current readout) within about 100 hr of operation.

An extended test was started with the TWT operating at saturation at 15 GHz. After about 400 hr of CW operation, the ion pump was turned off entirely. In retrospect, this could probably have been done at the start of the long-term test. The testing was continued until over 1200 hr of CW operation had been accumulated. A daily check was made for a possible pressure buildup by turning the pump back on for a few seconds; no measurable pump current was ever detected.

As discussed in the section MDC Assembly Design and Fabrication and as illustrated in figure 5, the MDC contained considerably more graphite material than actually required. Consequently, with a design which uses a minimum amount of graphite (such as illustrated in fig. 12), more rapid TWT-MDC processing could be expected. It is estimated that the "packaged" outer diameter of this collector could be reduced to 3.4 cm (from 4.6 cm) and the volume of graphite between an outer diameter of 3 cm and an inner diameter of 2 cm could be eliminated, thereby improving its outgassing performance.

Summary of TWT-MDC Performance Tests at Lewis

Pulsed performance data, individually optimized for each MDC, were obtained for all four TWT's under comparable operating conditions before CW operation was attempted. All

four TWT's were eventually brought up to CW operation. However, reliable CW data were obtained only with TWT's 203 and 204. In the case of TWT 201, a nonconstant electrical leakage in the MDC prevented an accurate determination of I_G and the overall efficiency η_{ov}. In the case of TWT 202, partial separation of the ceramic metallization film resulted in excessive overheating of electrode 3, which caused remelting and redeposition of braze material on the active portion of electrode 4, over a period of time. Consequently, the CW performance and the magnitude of the optimized MDC voltages of TWT 202 were found to be significantly different from the early pulsed results and were not considered as representative of the pyrolytic graphite MDC.

Extended CW testing was performed with TWT's 203 and 204 to examine the longer term stability of the collector electrode surfaces. Testing of TWT 203 included extended

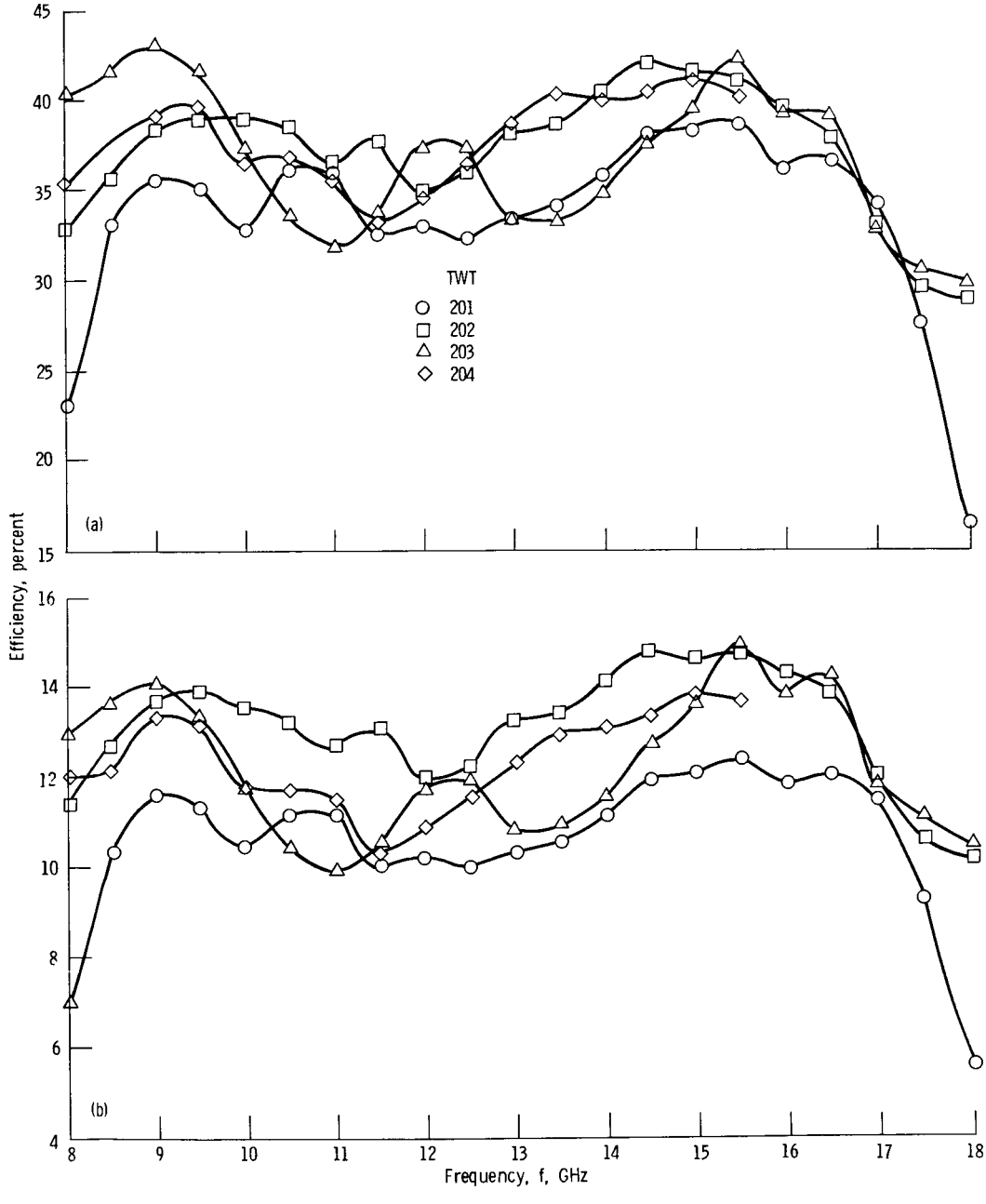

(a) Overall efficiency, η_{ov}.
(b) RF efficiency, η_{RF}.

Figure 13.—Overall and RF efficiencies as functions of frequency at saturation under similar operating conditions.

operation both with RF and with the dc beam. The latter produced particularly high incident current and energy dissipation on a single collector electrode.

Results of Pulsed Tests

Figure 13 shows the RF efficiency η_{RF} and η_{ov} as functions of frequency for the four TWT's. The TWT-MDC operating parameters are shown in table V. The data were obtained at a duty cycle of 50 percent with 1.0-msec pulses. TWT 204 had a high RF output voltage standing wave ratio (VSWR) above 16 GHz, and its useful operating band was limited to the range of 8 to 15.5 GHz. It is evident that these TWT's of identical design exhibited substantially different $\eta_{RF}(f)$ characteristics, and, therefore, almost certainly substantially different $P_b(f)$ characteristics, where P_b is the sum of beam interception losses and circuit losses. Consequently, as discussed in the section Performance Evaluation and Optimization Techniques, a determination and meaningful comparison of collector efficiencies was not possible. Each of the MDC's more than tripled η_{ov} as compared to that obtained without collector depression.

Results of CW Tests

The RF and TWT overall efficiencies as functions of frequency for TWT's 203 and 204 are shown in figure 14. The net dc input power as a function of frequency for the two TWT's is shown in figure 15. The overall efficiency as a function of η_{RF} at midband for TWT's 203 and 204 is shown in figure 16. These results were obtained early (after tens of hours) in the CW test program.

The MDC current distribution for operation of TWT 203 across its useful operating band of 8 to 18 GHz at saturation is shown in figure 17. The MDC current distribution as function of P_{RF} at midband is shown in figure 18. The collector current distribution of TWT 204 for operation at saturation from 8 to 15.5 GHz is shown in figure 19. The collector current distribution of TWT 204 as a function of P_{RF} at 13 GHz is shown in figure 20. The MDC voltages used are shown in table VI. These voltages, together with the maximum values of the current to the n^{th} collector electrode I_{en} define the power conditioning requirements of these TWT-MDC combinations.

TABLE V.—TWT-MDC OPERATING PARAMETERS OF TWT'S 201 TO 204 FOR BROADBAND PULSED OPERATION AT SATURATION

TWT parameter	TWT 201	TWT 202	TWT 203	TWT 204
Voltage on electrodes 1 to 4, kV				
V_{e1}	−4.75	−5.10	−4.85	−4.80
V_{e2}	−6.33	−6.05	−6.40	−6.60
V_{e3}	−7.32	−7.20	−7.52	−7.50
V_{e4}	−9.50	−9.60	−9.60	−9.60
Cathode voltage, V_0, kV	−9.50	−9.60	−9.60	−9.60
Cathode current, I_0, A	0.250	0.236	0.240	0.240

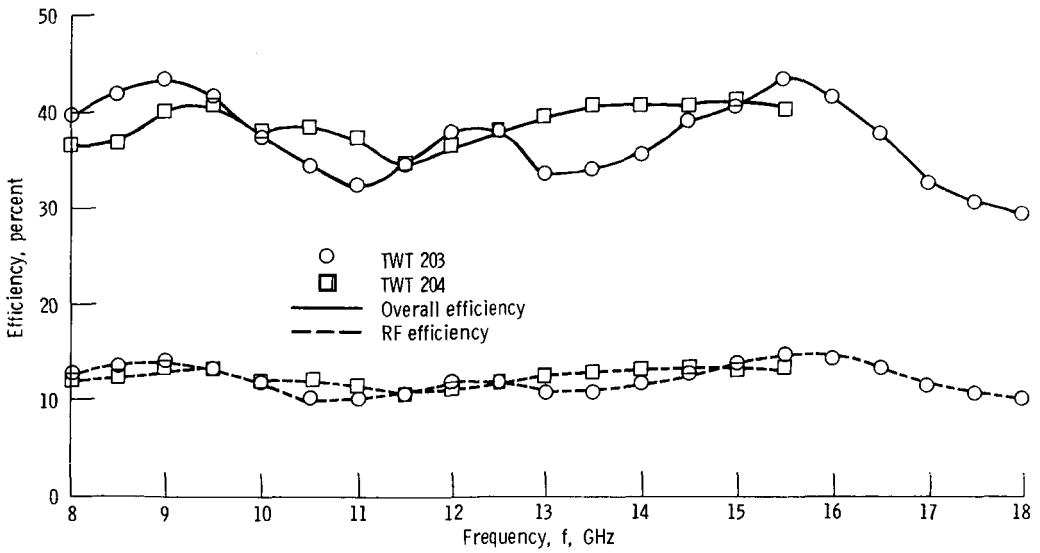

Figure 14.—Overall and RF efficiencies as functions of frequency for TWT's 203 and 204 under CW operating conditions. Cathode voltage, V_0, 9.6 kV; cathode current, I_0, 0.24 A.

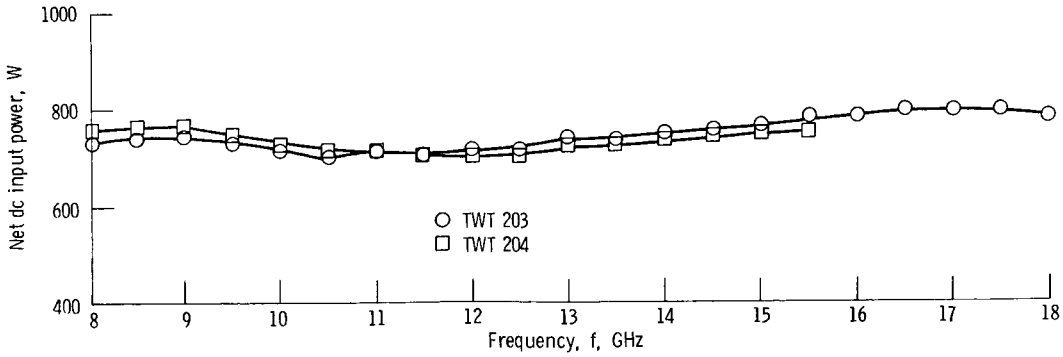

Figure 15.—Net dc input power as function of frequency for TWT's 203 and 204.

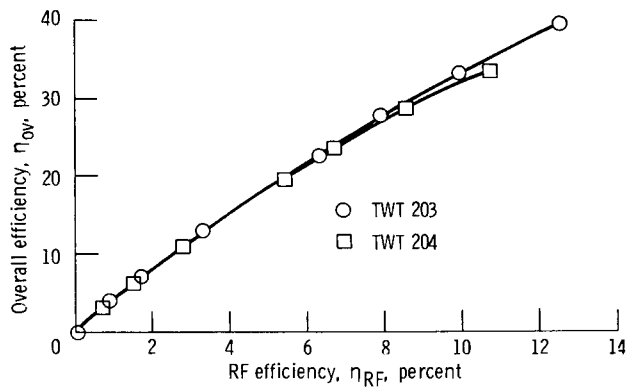

Figure 16.—Overall efficiency as function of RF efficiency for TWT's 203 and 204. Cathode voltage, V_0, 9.6 kV; cathode current, I_0, 0.24 A; frequency, f, 13 GHz.

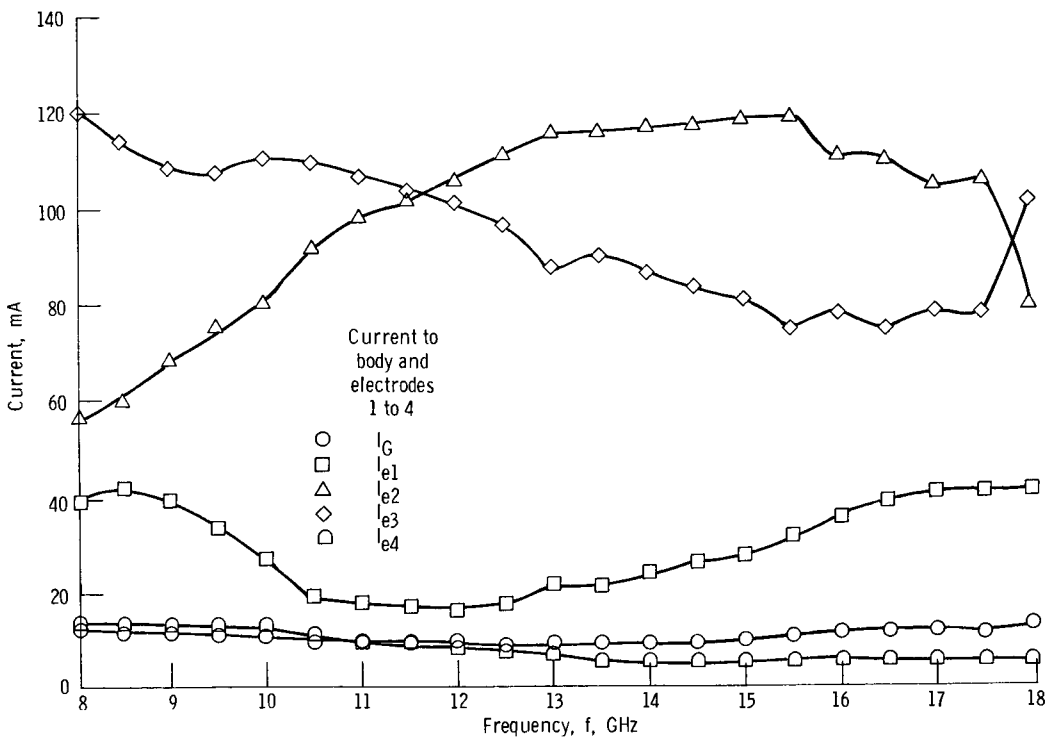

Figure 17.—Collector electrode current as function of frequency for TWT 203.

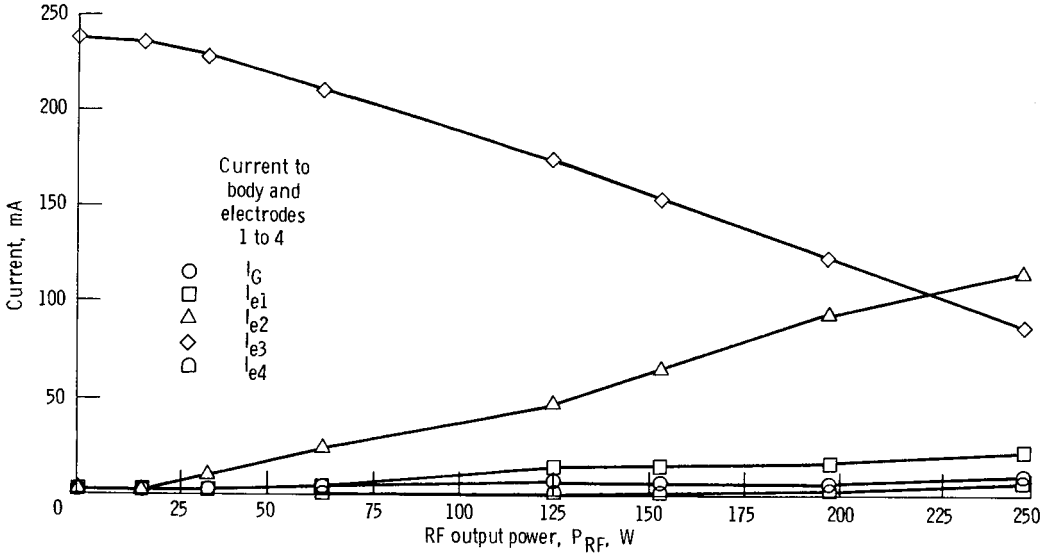

Figure 18.—Collector electrode current as function of RF output power for TWT 203. Frequency, f, 13 GHz.

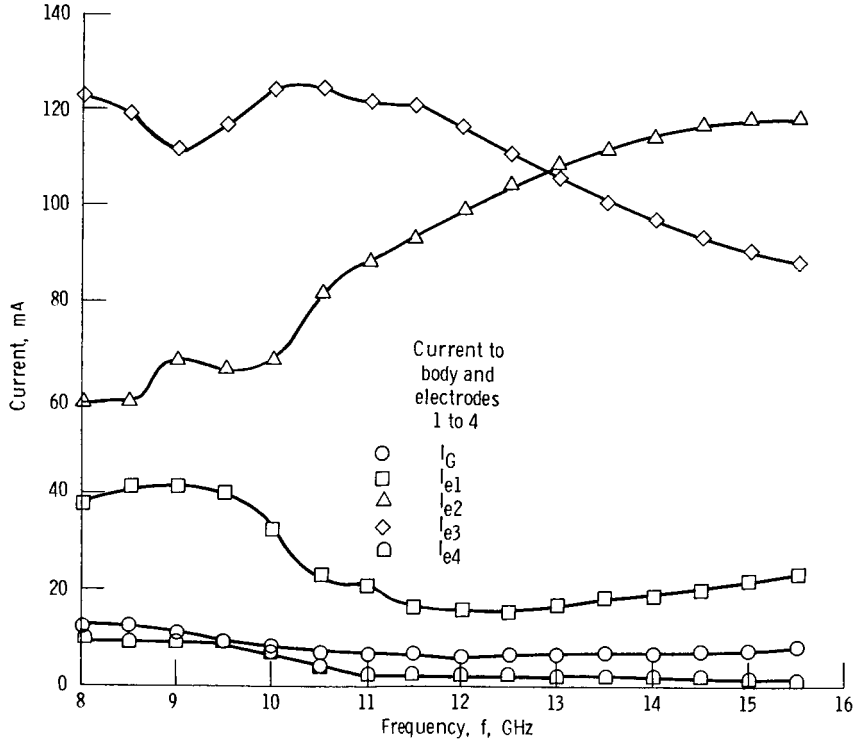

Figure 19.—Collector electrode current as function of frequency for TWT 204.

TABLE VI.—MDC OPERATING VOLTAGES OF TWT'S 203 AND 204 FOR BROAD-BAND CW OPERATION AT SATURATION

	TWT 203	TWT 204
Voltage on electrodes 1 to 4, kV		
V_{e1}	−4.80	−4.80
V_{e2}	−6.40	−6.40
V_{e3}	−7.50	−7.40
V_{e4}	−9.60	−9.60

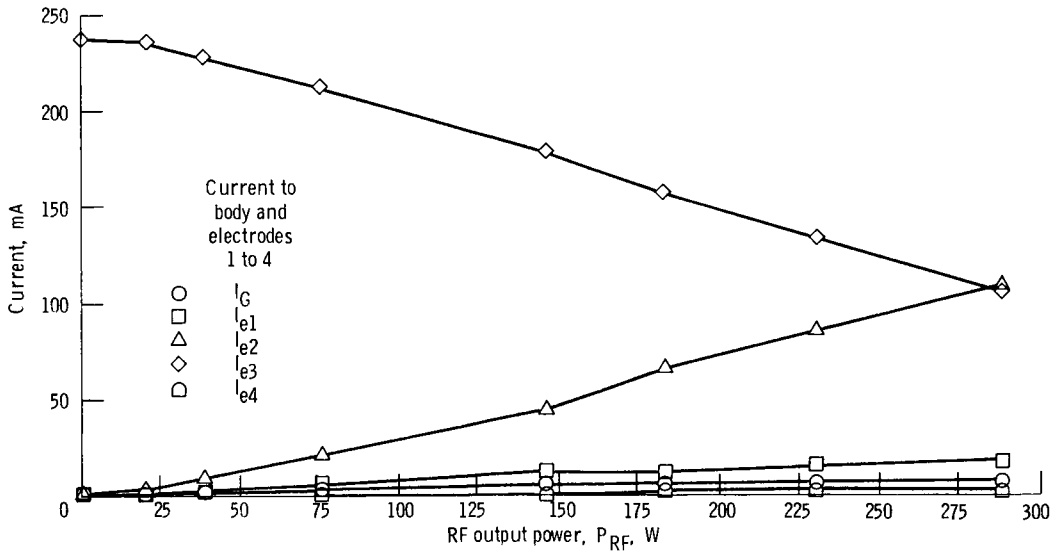

Figure 20.—Collector electrode current as function of RF output power for TWT 204. Frequency, f, 13 GHz.

Results of Extended CW Tests

The TWT 203 was operated CW for a total of about 2000 hr. The testing consisted of three phases. During the first 300 hr the TWT was operated at a variety of conditions to thoroughly outgas the MDC. This was followed by approximately 800 hr of operation at saturation at 9.0 GHz, after which the TWT-MDC performance across the operating band at saturation was reexamined. Shortly thereafter, the TWT began to exhibit an RF power fade, following an unscheduled shutdown due to a power outage. The third phase consisted of approximately 900 hr of operation with the dc beam.

Typical TWT-MDC operating conditions during the second and third phases are shown in table VII. The depression on electrode 3 was increased for operation with the dc beam to limit the power dissipation of electrode 3 to the design level (the optimized voltage on electrode 3 for broadband operation was substantially lower than the analytical design voltage as

TABLE VII.—TYPICAL OPERATING CONDITIONS OF TWT 203 DURING EXTENDED CW TEST

[Cathode voltage, V_0, 9.6 kV; cathode current, I_0, 0.24 A.]

TWT parameter	Operating condition	
	9.0 GHz, saturation	dc beam
Total RF output power, P_{RF}, W	320	0
Total body current, I_G, mA	10	3
Current to electrodes 1 to 4, mA		
I_{e1}	37	1
I_{e2}	71	1
I_{e3}	109	235
I_{e4}	13	0
Voltage on electrodes 1 to 4, V		
V_{e1}	−4800	−4800
V_{e2}	−6400	−6400
V_{e3}	−7500	−7950
V_{e4}	−9600	−9600

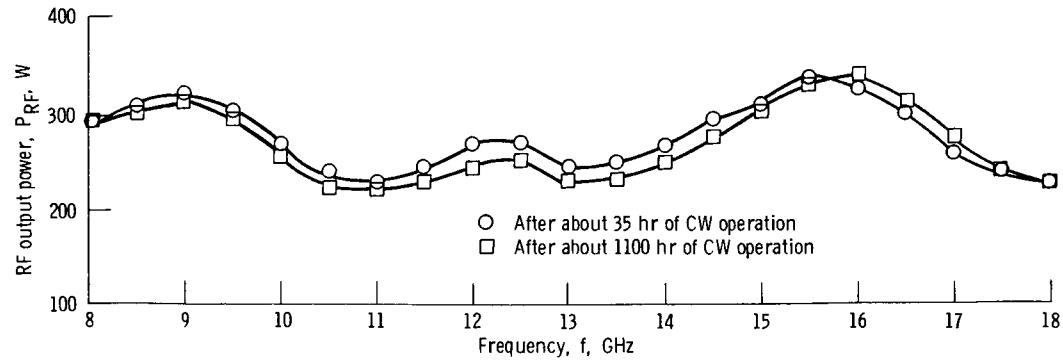

Figure 21.—RF output power as function of frequency at beginning and near end of CW RF test for TWT 203.

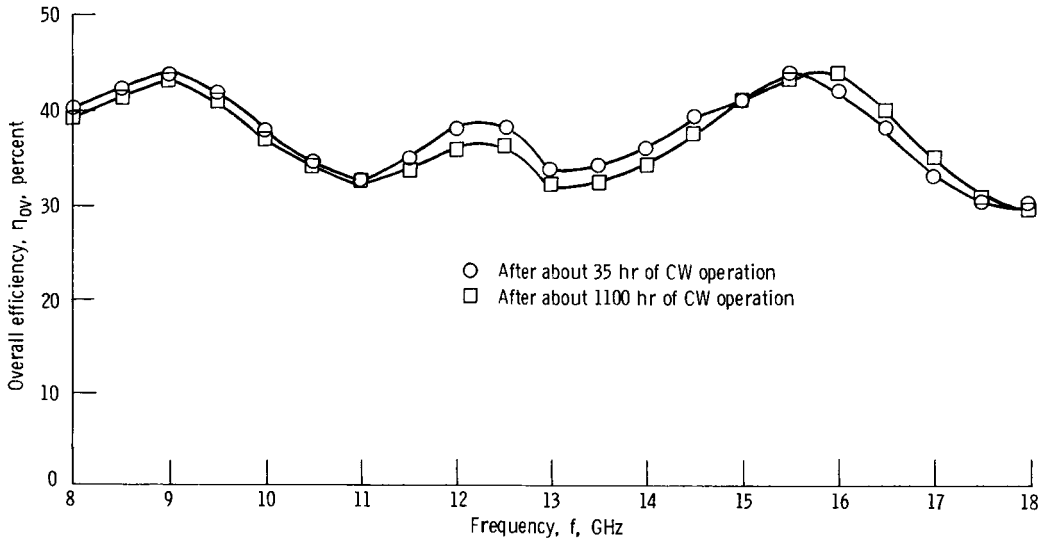

Figure 22.—Overall efficiency as function of frequency at beginning and near end of CW RF test for TWT 203.

discussed in ref. 2). The thermal dissipation on electrode 3 was at least 390 W during the dc beam test.

The TWT-MDC performances at approximately 35 and 1100 hr in the test are compared in figures 21 and 22. The RF efficiency was found to be somewhat lower over most of the operating band after extended operation. However, where the RF efficiencies were comparable the MDC performance was very similar. This is illustrated in table VIII for saturated operation at 17.5 and 18.0 GHz. The MDC performance at the beginning and end of the test with the dc beam is shown in table IX. No degradation whatsoever was observed in the MDC performance, and this demonstrates good stability of the textured pyrolytic graphite electrode surfaces. The observation was confirmed by scanning electron microscope examinations of selected areas of the electrodes before assembly of the MDC and after it was cut apart.

TWT 204 was operated CW for more than 1200 hr, mostly at saturation at 15 GHz. The typical operating condition is shown in table X.

During the first several hundred hours of operation, the body current rose (from 3 percent of the cathode current I_0 to 5 percent), and the recovered power P_{rec} dropped about 20 W, the largest changes occurring early in the extended test program. The RF output power remained constant within 1 percent, but the saturated gain increased slightly. The overall efficiency decreased by 1 to 1.5 percentage points. It could

TABLE VIII.—TWT-MDC PERFORMANCE EARLY IN CW TEST AND AT END OF EXTENDED CW RF TEST OF TWT 203

[Cathode voltage, V_0, 9.6 kV; cathode current, I_0, 0.24 A.]

(a) 17.5 GHz, saturation

TWT parameter	At $t \approx 35$ hr	At $t \approx 1100$ hr
Total RF output power, P_{RF}, W	244	240
Total body current, I_G, mA	11	10
Current to electrodes 1 to 4, mA		
I_{e1}	41	41
I_{e2}	106	110
I_{e3}	78	74
I_{e4}	5	6
Recovered power, P_{rec}, W	1507	1510
Total dc input power, W	798	794
Overall efficiency, η_{ov} percent	30.6	30.3

(b) 18.0 GHz, saturation

TWT parameter	At $t \approx 35$ hr	At $t \approx 1100$ hr
Total RF output power, P_{RF}, W	231	231
Total body current, I_G, mA	13	10
Current to electrodes 1 to 4, mA		
I_{e1}	41	41
I_{e2}	80	90
I_{e3}	102	94
I_{e4}	6	5
Recovered power, P_{rec}, W	1522	1527
Total dc input power, W	784	777
Overall efficiency, η_{ov} percent	29.4	29.8

TABLE IX.—TWT-MDC PERFORMANCE OF TWT 203 AT START AND END OF CW TEST WITH dc BEAM

[Cathode voltage, V_0, 9.6 kV; cathode current, I_0, 0.24 A.]

TWT parameter	At $t \approx 1125$ hr	At $t \approx 2000$ hr
Total RF output power, P_{RF}, W	0	0
Total body current, I_G, mA	4	3
Current to electrodes 1 to 4, mA		
I_{e1}	2	1
I_{e2}	2	1
I_{e3}	232	235
I_{e4}	0	0
Total dc input power, W	435	421

TABLE X.—TYPICAL TWT-MDC OPERATING CONDITIONS DURING EXTENDED CW TEST OF TWT 204

[Cathode voltage, V_0, 9.6 kV; cathode current, I_0, 0.24 A; frequency, f, 15 GHz.]

Total RF output power, P_{RF}, W	314
Total body current, I_G, mA	8
Current to electrodes 1 to 4, mA	
I_{e1}	23
I_{e2}	116
I_{e3}	92
I_{e4}	1
Total dc input power, W	760

not be definitely established whether the changes in body current and recovered power were due to changes in the TWT itself (larger beam due to improved outgassing of the TWT components), to small dimensional changes in the TWT or MDC, or to changes in the secondary-electron-emission characteristics of the graphite electrodes.

Examination of the collector electrode surfaces was not possible since the TWT-MDC was kept intact for possible additional testing.

Concluding Remarks

Very small pyrolytic graphite and isotropic graphite electrode MDC's were extensively tested in conjunction with medium-power TWT's. Preliminary results indicate that some additional RF and dc beam processing time and/or longer or higher temperature bakeouts may be needed than for typical copper electrode collectors. This is particularly true for TWT's that do not use appendage ion pumps and for the pyrolytic graphite MDC's, which exhibited very low level but persistent outgassing even after extensive operation.

For lower power space TWT's, reduced operating temperatures of the graphite electrodes should reduce the processing time. For higher power applications, use of beryllium oxide collector insulators in place of the alumina used here is indicated.

The isotropic graphite in particular was found to show considerable promise as an MDC electrode material because of the following characteristics:

(1) High purity
(2) Low cost and ready availability
(3) Simple, lower cost construction
(4) Compact overall size
(5) Relatively low secondary-electron-emission characteristics in the as-machined state

However, considerably more experience with isotropic graphite in MDC's is required before definitive conclusions on its suitability for ECM systems and space TWT's can be made.

National Aeronautics and Space Administration
Lewis Research Center
Cleveland, Ohio, November 26, 1986

References

1. Ramins, P.; Ebihara, B.T.: Secondary-Electron-Emission Losses in Multistage Depressed Collectors and Traveling-Wave-Tube Efficiency Improvements with Carbon Collector Electrode Surfaces. NASA TP-2622, 1986.
2. Ramins, P., et al.: Verification of Computer-Aided Designs of Traveling-Wave Tube Utilizing Novel Dynamic Refocusers and Graphite Electrodes for the Multistage Depressed Collectors. NASA TP-2524, 1985.
3. Curren, A.N.; and Jensen, K.A.: Beam Impingement Angle Effects on Secondary Electron Emission Characteristics of Textured Pyrolytic Graphite. NASA TP-2285, 1984.
4. Smith, W.H.; and Leeds, D.H.: Pyrolytic Graphite. Modern Materials; Advances in Development and Applications, Vol. 7, B.W. Gosner, ed., Academic Press, 1970, pp. 139–221.
5. Ebihara, B.T.: Multistage Spent Particle Collector and a Method for Making Same. U.S. Patent 4,527,092, July, 1985.
6. Wilkins, W.J.: Pyrolytic Graphite Collector Development Program. (W-01970, Hughes Aircraft Co.; NASA Contract NAS3-22505) NASA CR-167909, 1982.

1. Report No.	2. Government Accession No.	3. Recipient's Catalog No.
NASA TP-2693		

4. Title and Subtitle	5. Report Date
Design, Fabrication, and Performance of Small, Graphite Electrode, Multistage Depressed Collectors With 200-W, CW, 8- to 18-GHz Traveling-Wave Tubes	February 1987
	6. Performing Organization Code: 506-44-21
7. Author(s): Ben T. Ebihara and Peter Ramins	8. Performing Organization Report No.: E-3099
	10. Work Unit No.
9. Performing Organization Name and Address: National Aeronautics and Space Administration, Lewis Research Center, Cleveland, Ohio 44135	11. Contract or Grant No.
	13. Type of Report and Period Covered: Technical Paper
12. Sponsoring Agency Name and Address: National Aeronautics and Space Administration, Washington, D.C. 20546	14. Sponsoring Agency Code

15. Supplementary Notes

16. Abstract

Small multistage depressed collectors (MDC's) which used pyrolytic graphite, ion-beam-textured pyrolytic graphite, and isotropic graphite electrodes were designed, fabricated, and evaluated in conjunction with 200-W, continuous wave (CW), 8- to 18-GHz traveling-wave tubes (TWT's). The design, construction, and performance of the MDC's are described. The bakeout performance of the collectors, in terms of gas evolution, was indistinguishable from that of typical production tubes with copper collectors. However, preliminary results indicate that some additional radiofrequency (RF) and dc beam processing time (and/or longer or higher temperature bakeouts) may be needed beyond that of typical copper electrode collectors. This is particularly true for pyrolytic graphite electrodes and for TWT's that do not have appendage ion pumps. Extended testing indicated good long-term stability of the textured pyrolytic graphite and isotropic graphite electrode surfaces. The isotropic graphite in particular showed considerable promise as an MDC electrode material because of its high purity, low cost, simple construction, potential for very compact overall size, and relatively low secondary-electron-emission yield characteristics in the as-machined state. However, considerably more testing experience is required before definitive conclusions on its suitability for electronic countermeasure systems and space TWT's can be made.

17. Key Words (Suggested by Author(s))	18. Distribution Statement
Collector design; Collector; Collector performance; Secondary electron suppression; Graphite	Unclassified – unlimited STAR Category 33

19. Security Classif. (of this report)	20. Security Classif. (of this page)	21. No of pages	22. Price*
Unclassified	Unclassified	21	A02

*For sale by the National Technical Information Service, Springfield, Virginia 22161

NASA-Langley, 1987